

Magnetic and Electron Spin Resonance Properties of $\text{Ba}_x\text{Sr}_{2-x}\text{TiCoO}_6$ Double Perovskites

Deepankar Sri Gyan, Mandvi Saxena, Rushana Eremina, Ilshat Fazlizhanov, Dzhavid Mamedov, Ivan Yatsyk, Ashutosh Kumar Shukla, Akansha Dwivedi, and Tanmoy Maiti*

Herein, the magnetic behavior of $\text{Ba}_x\text{Sr}_{2-x}\text{TiCoO}_6$ (BSTC) double perovskites synthesized by the conventional solid-state reaction route is investigated. To understand the complexity of B-site cations and their distribution in different valance states, X-ray photoelectron spectroscopy (XPS) is performed. To understand the magnetic interactions at lower temperatures, variation of magnetization in both zero-field-cooled and field-cooled conditions is studied in the temperature range from 2 to 300 K. Temperature dependence of inverse susceptibility is explained by modified Curie–Weiss law. Weak ferromagnetic and antiferromagnetic interactions are found in BSTC compounds, causing the randomness and frustrations and leading to a spin-glass-like behavior. To gain further insights, electron spin resonance (ESR) measurements are also carried out in BSTC ceramics. ESR measurement suggests the occurrence of Jahn–Teller glass analogous to the spin-glass behavior in BSTC ceramics.

1. Introduction

Double perovskite oxides has been a fascinating research topic in the past few decades, due to their intriguing magnetic, electrical,

dielectric, and colossal magnetoresistance properties.^[1–3] Moreover, these double perovskites also displayed interesting properties like transition from insulating to metallic or even half metallic.^[4,5] The general formula of double perovskite is $\text{A}_2\text{B}'\text{B}''\text{O}_6$, where A is a divalent alkaline earth metal and B' and B'' represent transition metals. The schematic of cubic double perovskite with a random octahedral arrangement is shown in **Figure 1a**. The interaction between two transition metals or even the same metals with different valence states induces new exchanges, resulting in interesting magnetic properties.^[6–8] It was reported that when the B-site was occupied by both ferromagnetic and nonferromagnetic metals, double perovskites exhibited a wide range of magnetic behaviors such as antiferromagnetism,^[9] ferromagnetism,^[10] magnetic frustration,^[11] colossal magnetoresistance,^[1,2] multiferroicity,^[12] etc. $\text{Sr}_2\text{FeMoO}_6$ -based double perovskites were reported to possess colossal magnetoresistance-type half-metallic ferromagnetic behavior with ≈ 415 K Curie temperature.^[2] On the contrary, $\text{Sr}_2\text{CoMoO}_6$ showed an insulating antiferromagnetic behavior ($T_N = 37$ K) and converted into semiconductor ferromagnetic upon chemical reduction.^[1] Moreover, some other double perovskites demonstrated antiferromagnetic behavior at a low temperature depending on the combination of cations.^[8]

In the current investigation, efforts have been made to understand the magnetic behavior of Ba-doped $\text{Sr}_2\text{TiCoO}_6$ (STC) double perovskite, in which B-site is occupied by the ferromagnetic Co ion and nonferromagnetic Ti ion.^[13] STC double perovskite has appeared to be an interesting material because it is a combination of SrTiO_3 , a band insulator,^[14] and SrCoO_3 , a ferromagnetic material.^[15] Our group recently reported that the thermoelectric performance of the p-type polycrystalline STC double perovskites could be enhanced by barium doping.^[13] These ceramics exhibited a high Seebeck coefficient and low thermal conductivity. Glass-like thermal conductivity of these double perovskites was attributed to their low-temperature relaxor ferroelectric behavior, following Vogel–Fulcher Law, which was originally derived for spin glass.^[16] Therefore, it is intriguing to study the magnetic behavior of $\text{Ba}_x\text{Sr}_{2-x}\text{TiCoO}_6$ (BSTC) double perovskites. Trivalent Co^{3+} is found to be stabilized in low-spin (LS) (t_{2g}^6), intermediate-spin (IS) ($t_{2g}^5e_g^1$), as well as high-spin (HS) ($t_{2g}^4e_g^2$) states. If HS magnetic ions are


D. Sri Gyan, Dr. M. Saxena, Dr. A. K. Shukla, Dr. T. Maiti
Plasmonics and Perovskites Laboratory
Indian Institute of Technology Kanpur
Kanpur 208016, UP, India
E-mail: tmaiti@iitk.ac.in

D. Sri Gyan, Dr. A. Dwivedi
Department of Ceramic Engineering
Indian Institute of Technology (BHU)
Varanasi 221005, UP, India

Dr. R. Eremina, Dr. I. Fazlizhanov, Dr. D. Mamedov, Dr. I. Yatsyk
Zavoisky Physical-Technical Institute
FRC Kazan Scientific Center of RAS
Sibirsky tract, 10/7, Kazan 420029, Russia

Dr. A. K. Shukla
Physics Department
Ewing Christian College
Allahabad 211003, UP, India

Dr. M. Saxena, Dr. T. Maiti
Department of Materials Science and Engineering
Indian Institute of Technology Kanpur
Kanpur 208016, UP, India

 The ORCID identification number(s) for the author(s) of this article can be found under <https://doi.org/10.1002/pssb.201900341>.

DOI: 10.1002/pssb.201900341

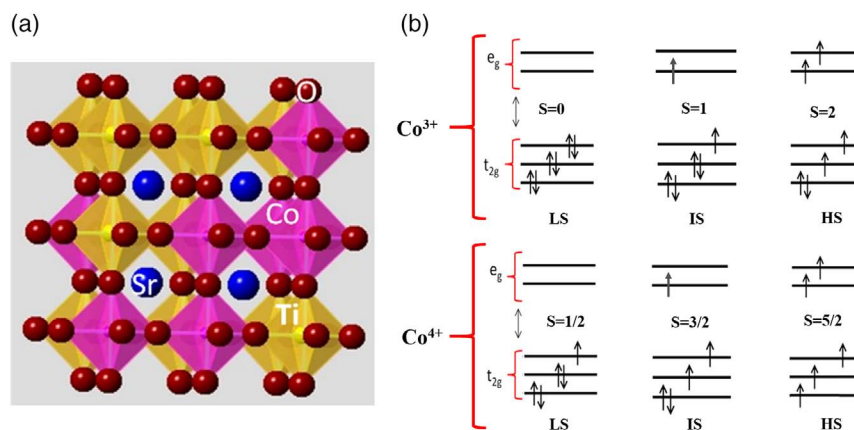


Figure 1. a) The schematic of the cubic structure of Sr₂TiCoO₆ with randomly oriented TiO₆ and CoO₆ octahedra. b) A schematic of the idealized spin states on the octahedral-oriented Co-cation: LS, IS, and HS states.

present as neighbors of the Co ion, Co³⁺ tends to possess a HS state by double exchange interaction.^[15] However, in the case of STC, as the neighboring ions are nonmagnetic Ti, trivalent Co³⁺ is likely to possess t_{2g}⁶ LS state.^[17] Co³⁺ with an LS state has no unpaired electron and therefore behaves like diamagnetic. However, LS of Co⁴⁺ has a single unpaired electron. Figure 1b shows the schematic of idealized spin states of the octahedral-oriented Co ion in both LS and HS states.

In this work, we have studied the low-temperature magnetic behavior of BSTC ($x = 0, 0.1, \text{ and } 0.2$) ceramics. To the best of our knowledge, there are no reports on the magnetic behavior of BSTC ceramics. The variation of magnetization with temperature has been measured in the temperature range from 2 to 300 K, and M – H hysteresis loops have been traced for $x = 0$ and 0.2 compositions at 2 K. The electron spin resonance (ESR) measurements have been carried out from room temperature to 700 K. Moreover, to understand the distribution of the oxidation states of Co and Ti, X-ray photoelectron spectroscopy (XPS) has been conducted at room temperature. An interesting spin-glass behavior has been observed in BSTC ceramics.

2. Results and Discussion

2.1. Structural Analysis

Authors have already reported^[13] the structural and microstructural analyses of BSTC ceramics. X-ray powder diffraction (XRD) of these ceramics shows single-phase solid solution. Furthermore, the crystal structure of these double perovskites has been found to be cubic with Pm $\bar{3}$ m space group via Rietveld refinement of room-temperature XRD data, as shown in Figure 2a. Moreover, scanning electron microscopy (SEM) of these compositions demonstrates the dense microstructure with no such porosity, as shown in Figure 2b. Figure 2c–f shows the elemental mapping of Sr, Co, Ti, and O elements conducted by energy-dispersive X-ray spectroscopy (EDXS). It is evident from the figure (c–f) that all the constituent elements are homogeneously distributed throughout the STC ceramic sample.

Furthermore, to check the high-temperature stability of these ceramics, we have performed thermal gravimetric analysis (TGA), as shown in Figure 3a, for BSTC with $x = 0$ and 0.2 compositions in reducing atmosphere (10% H₂ + Ar). As shown in the figure, these compositions exhibit a negligible amount (<1%) of weight loss up to 900 K, suggesting excellent stability of STC compounds at high temperatures. This weight loss is attributed as oxygen loss because the experimental condition was reducing. Therefore, it can be extrapolated to calculate stoichiometric loss in oxygen by estimating δ in Ba _{x} Sr_{1– x} TiCoO_{6– δ} . Figure 3a also shows the variation of δ with temperature and it is found to be 0.24 for $x = 0.2$ sample at 1073 K. It is reasonable for perovskite structure to hold with this amount of stoichiometric loss. It is to be noted that TGA was conducted in reducing atmosphere, whereas measurements of conductivity and magnetic properties were carried out in a vacuum condition where oxygen loss might be very low. Also, the primary focus of the current work is to discuss the magnetic behavior of this ceramic at a low-temperature region below 300 K, where BSTC is expected to have much lower oxygen vacancies. Furthermore, we have conducted the high-temperature XRD of STC composition, as shown in Figure 3b. It is shown from the XRD graph that these materials demonstrate single-phase solid solution in the temperature range from 300 to 973 K as no such extra peaks corresponding to any secondary phase have been detected. Therefore, it can be concluded that BSTC ceramics are quite stable even at high temperatures.

2.2. XPS

To find out the oxidation states of Co and Ti in double perovskite, XPS has been conducted. Figure 4 shows the high-resolution XPS spectra for the Ba_{0.2}Sr_{1.8}TiCoO₆ ceramic sample, demonstrating Ti 2p and Co 3p peaks, fitted using Lorentzian–Gaussian line shapes. The existence of the mixed valence states of Ti⁴⁺ and Ti³⁺ is clearly evident from the fitting patterns of XPS spectra of BSTC with $x = 0.2$ sample, as shown in Figure 4a. The binding energies for Ti⁴⁺ 3p_{3/2;1/2} and Ti³⁺ 3p_{3/2;1/2} (Table 1) are close to the reported values in the

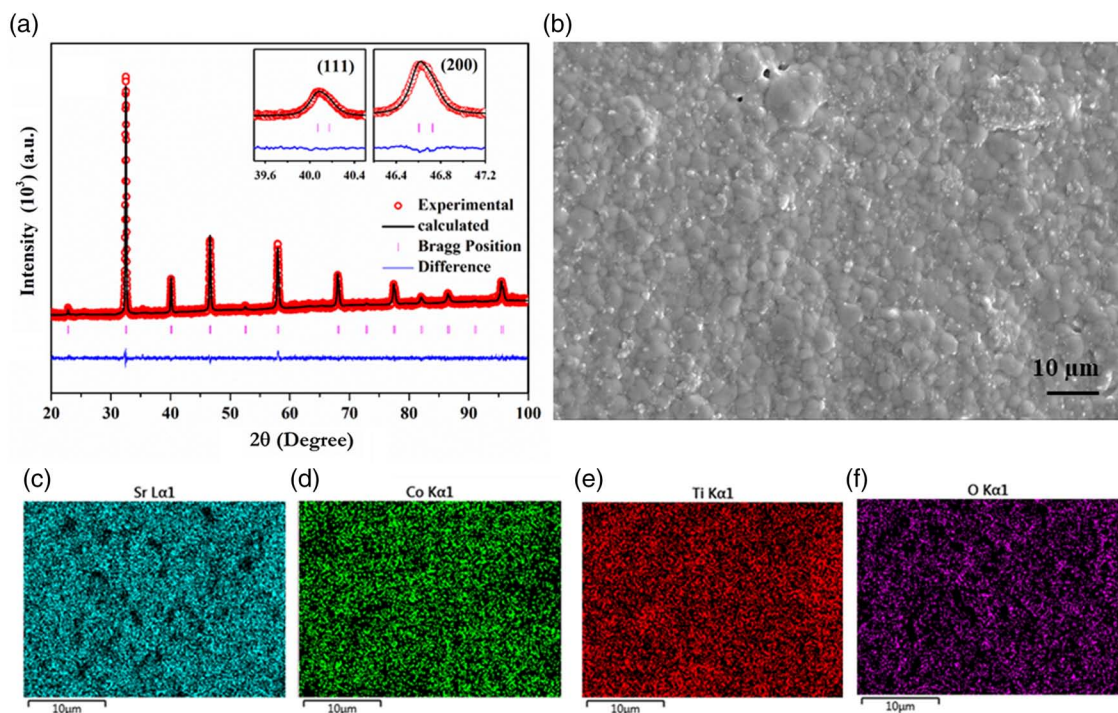


Figure 2. a) Rietveld refinement of XRD data ($R_B = 1.45$, R_F factor = 1.54, $\chi^2 = 1.41$); b) SEM micrograph; EDS mapping of c) Sr, d) Co, e) Ti, and f) O elements of STC ceramics.

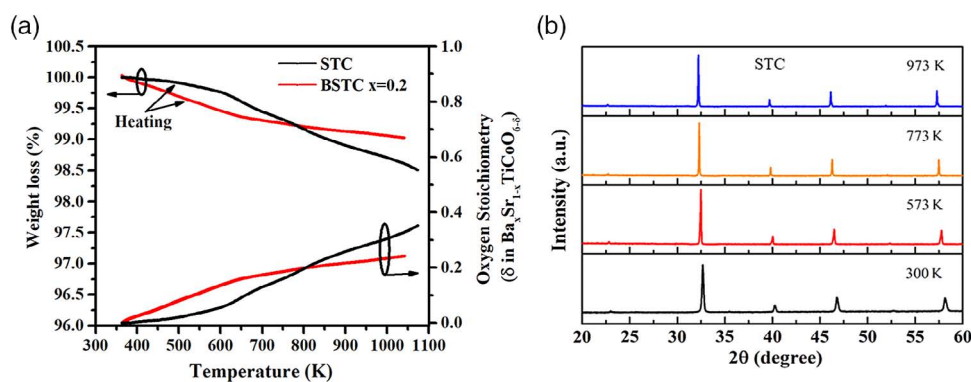


Figure 3. a) Weight loss (%) from TGA and stoichiometric loss in oxygen due to temperature rise (δ in $Ba_xSr_{1-x}TiCoO_{6-\delta}$) and b) high-temperature XRD of STC ceramic.

literature.^[18,19] It is evident from the data shown in Table 2 that the area % of Ti^{4+} is higher as compared with Ti^{3+} , which suggests that most of Ti has a tendency to acquire +4 valance state instead of +3. To estimate the valance state of Co, the Co 2p peak of XPS spectra has also been fitted using Lorentzian–Gaussian line shapes, as shown in Figure 4b. Two peaks located ≈ 780 and 795 eV correspond to Co $2p_{3/2}$ and Co $2p_{1/2}$, respectively. The binding energies of these peaks have been found to match well with the literature.^[20–22] Co has been found to possess Co^{3+} and Co^{4+} oxidation states in our BSTC samples. $Co^{3+} 2p_{3/2;1/2}$ and $Co^{4+} 2p_{3/2;1/2}$ have been observed at binding energies of 780.22; 795.46 eV and 781.37; 796.56 eV, respectively. The satellite peaks of $2p_{3/2}$ and $2p_{1/2}$ have been obtained at binding

energies of 786.90 and 803.28 eV, respectively, similar to the other reports in the literature.^[20–23] The area corresponding to Co^{3+} and Co^{4+} peaks suggests 2:1 distribution of +3 and +4 valance states, in the ceramic double perovskites.

Due to the existence of Co^{3+} and Ti^{3+} in the B-site of double perovskite having a formal valance of +4, it is expected to have an oxygen-deficient compound of $Ba_{0.2}Sr_{1.8}TiCoO_{6-\delta}$. The value of δ for the as-synthesized double perovskite ceramic, $Ba_{0.2}Sr_{1.8}TiCoO_{6-\delta}$, calculated using XPS data has been found to be 0.92. Adding to the oxygen loss due to increase in temperatures, calculated from TGA data, the δ value can be around 1.16 at 973 K. With such a large amount of oxygen vacancies, it may be difficult to hold the perovskite structure. However,

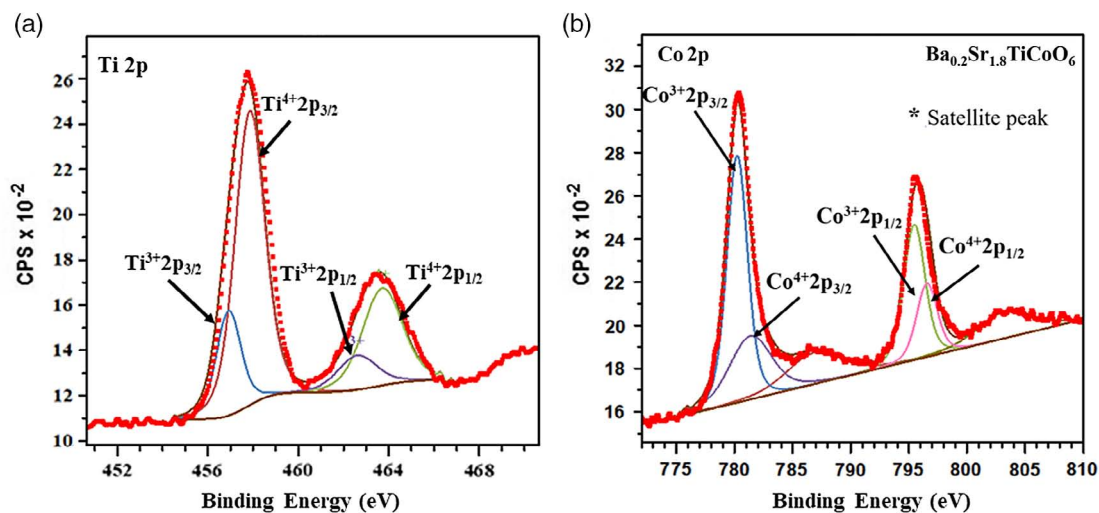


Figure 4. XPS analysis of a) Ti and b) Co for $\text{Ba}_{0.2}\text{Sr}_{1.8}\text{TiCoO}_6$ ceramics.

Table 1. Binding energy and area % of titanium and cobalt for $\text{Ba}_{0.2}\text{Sr}_{1.8}\text{TiCoO}_6$.

Element	State	Binding energy [eV]	Area [%]
Titanium	$\text{Ti}^{3+} 2p_{3/2}$	456.92	15.62
	$\text{Ti}^{3+} 2p_{1/2}$	462.60	8.12
	$\text{Ti}^{4+} 2p_{3/2}$	457.86	52.96
	$\text{Ti}^{4+} 2p_{1/2}$	463.82	23.31
Cobalt	$\text{Co}^{3+} 2p_{3/2}$	780.22	33.16
	$\text{Co}^{3+} 2p_{1/2}$	795.46	18.86
	$\text{Co}^{4+} 2p_{3/2}$	781.37	17.32
	$\text{Co}^{4+} 2p_{1/2}$	796.56	9.85
	Satellite $2p_{3/2}$	786.90	11.40
	Satellite $2p_{1/2}$	803.28	9.41

Table 2. Curie constant C , Weiss temperature θ , temperature-independent contribution χ_0 values obtained by fitting modified Curie–Weiss law with the experimental DC magnetic susceptibility.

Composition	C [$\mu\text{m}^2 \text{K mol}^{-1}$]	Θ [K]	χ_0 [$\mu\text{m}^2 \text{mol}^{-1}$]
$x = 0$	0.76	−12.4	1.33×10^{-5}
$x = 0.1$	0.74	−11.3	2.66×10^{-6}
$x = 0.2$	1.15	−6.1	3.98×10^{-6}

several double perovskites were reported in the literature to exhibit a perovskite structure despite having a large amount of oxygen vacancies such as $\text{YBaCuFeO}_{5+\delta}$, $\text{PrBaCuFeO}_{5+\delta}$, $\text{LuBaCuFeO}_{5+\delta}$, and $\text{LaBaFeCuO}_{5+\delta}$.^[24–27] So, it might be possible for the system to have such a high value of δ . Furthermore, high-temperature XRD results (Figure 3b) clearly indicate that the single-phase perovskite structure is stabilized and holds up to at least 973 K, which the TGA result reconfirms as well. It is to be noted here that the calculation of delta (δ)

for $\text{Ba}_{0.2}\text{Sr}_{1.8}\text{TiCoO}_{6-\delta}$ may not be accurate because XPS is a surface-sensitive technique.

2.3. Magnetic Measurement of BSTC Double Perovskite Sample

DC magnetization for BSTC ($x = 0, 0.1, \text{ and } 0.2$) ceramic samples has been measured in the temperature range from 2 to 300 K. Plots of zero field cooled (ZFC) and field cooled (FC) magnetization and inverse of susceptibility ($1/\chi$) with temperature are shown in Figure 5. In the ZFC condition, the sample was first cooled down to 2 K in the absence of an external field and then the temperature was raised to 300 K in the presence of the magnetic field, 300 Oe. On the contrary, in FC, external field (300 Oe) was applied during both cooling and heating cycles. The net magnetization has shown an increasing trend with decreasing temperature, as shown in Figure 5a. Two striking features evident from the presented data are weak irreversibility between $M_{\text{ZFC}}(T)$ and $M_{\text{FC}}(T)$ curves and a hump in $M_{\text{ZFC}}(T)$ curve below 50 K around T_m , which is defined by the temperature corresponding with the maximum value of magnetization in the ZFC measurement. This hump around 50 K can be due to the local freezing of magnetic moments. This behavior is similar to a typical spin-glass state that emerged due to random freezing of magnetic moments at low temperatures.^[28–30] It can be observed from the M – T plots, shown in Figure 5, that $x = 0$ and 0.1 compositions have shown almost the same value of magnetization, whereas $x = 0.2$ composition has demonstrated slight increment in the net magnetization value.

Figure 5b shows the plot of inverse susceptibility ($1/\chi$) versus temperature (T). It is apparent that for the entire range of temperature, BSTC compositions do not follow the classical Curie–Weiss law ($\chi = C/(T - \theta)$), where C and θ are the Curie constant and Weiss temperature, respectively. Instead, it is only valid for the higher temperature range. Here, $C = \frac{N\mu_{\text{eff}}^2}{3k_B}$, where N is the number of Co ions/ m^3 and μ_{eff} is effective numbers of Bohr magneton given by $\mu_{\text{eff}} = g[J(J + 1)]^{1/2}\mu_B$; J is the spin quantum number and g is Landé g factor.^[31] The slope of the fitting gives the value of average spin (S_{avg}) in the material.^[31]

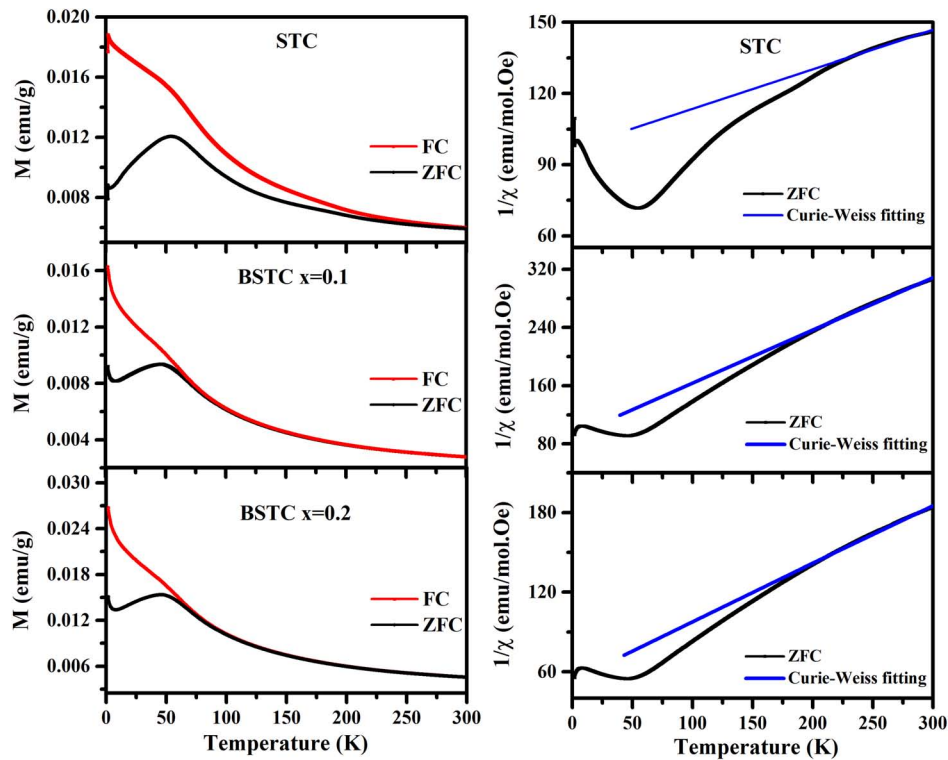


Figure 5. The temperature variation of the a) magnetization (M) and b) inverse susceptibility ($1/\chi$) fitted with Curie–Weiss law for BSTC ($x = 0, 0.1,$ and 0.2) ceramic samples.

Now, based on XPS analysis for the $x = 0.2$ composition, it has been predicted that 75% of Ti is present as Ti^{4+} , whereas rest 25% is Ti^{3+} . Also, 67% of Co is present as Co^{3+} , whereas rest 33% is Co^{4+} . So, if we consider these B-sites in $\text{A}_2\text{B}'\text{B}''\text{O}_6$ double perovskites as one mole, the material will have 0.375 moles Ti^{4+} , 0.125 moles Ti^{3+} , 0.335 moles Co^{3+} , and 0.165 moles Co^{4+} . Now based on this information, the average spin of the system can be expressed as

$$S_{\text{avg}} = 0.125 \times S^{\text{Ti}^{3+}} + 0.375 \times S^{\text{Ti}^{4+}} + 0.335 \times S^{\text{Co}^{3+}} + 0.165 \times S^{\text{Co}^{4+}} \quad (1)$$

where S^i is spin of ion i , $S^{\text{Ti}^{4+}}$ is always going to be zero, and $S^{\text{Ti}^{3+}}$ is always going to be 0.5 (as electronic configuration of Ti is $[\text{Ar}] 3d^2 4s^2$). Then, the resulting expression will be

$$S_{\text{avg}} = 0.0625 + 0.335 \times S^{\text{Co}^{3+}} + 0.165 \times S^{\text{Co}^{4+}} \quad (2)$$

Now, Co ions can reside in multiple states, as shown in Figure 1b. From the Curie–Weiss fitting of the data, as shown in Figure 5, S_{avg} has been estimated as 0.46. So, the final relation between spins of Co^{3+} and Co^{4+} is given by $0.335 \times S^{\text{Co}^{3+}} + 0.165 \times S^{\text{Co}^{4+}} = 0.3975$.

To begin with, let us assume Co^{3+} is present in a LS state, i.e., $S^{\text{Co}^{3+}} = 0$. This will lead to the situation where $S^{\text{Co}^{4+}} = 2.4$, which is very close to the spin state of Co^{4+} in high spin (2.5). But majority of Ti is present as the nonmagnetic Ti^{4+} state, and it is highly unlikely for Co to attain a high spin configuration when surrounded by a nonmagnetic ion.^[17] Now, let us suppose

Co^{4+} acquires a LS state, i.e., $S^{\text{Co}^{4+}} = 1/2$. This will lead to the situation where $S^{\text{Co}^{3+}} = 0.95$, which is close to 1. This means that Co^{3+} will tend to reside in the IS state. All the other combinations will never satisfy the aforementioned equation. Therefore, the most likely scenario is Co^{3+} ($t_{2g}^5 e_g^1$) having an IS state, whereas Co^{4+} ($t_{2g}^5 e_g^0$) has an LS state.

Furthermore, the deviation from Curie–Weiss law has been explained using modified Curie–Weiss law,^[32] expressed by $\chi = \chi_0 + C/(T - \theta)$, where χ_0 represents a term reflecting the Pauli susceptibility. Figure 6 shows the fitting of the modified Curie–Weiss law for BSTC with $x = 0, 0.1,$ and 0.2 , and the fitting parameters are shown in Table 2. Negative values of Weiss temperature θ have been obtained for all the samples, which have been reported in the literature as the signature of antiferromagnetic-type coupling.^[33]

Such antiferromagnetic coupling can be understood by considering the oxidation state of cobalt. XPS analysis suggested the presence of +3 and +4 oxidation states for Co. Generally, cobalt stabilizes in a LS state at a low temperature when it is surrounded by a nonmagnetic element (Ti) present in the material. In the LS state, Co^{4+} possesses one unpaired electron, which would give rise to antiferromagnetic-type coupling, due to the superexchange interaction between spin $\text{Co}^{4+}\text{--O--Co}^{4+}$.^[34] Also, there is antiferromagnetic-type coupling due to $\text{Co}^{3+}\text{--O--Co}^{3+}$ superexchange.^[34] However, the presence of a weak ferromagnetic interaction due to the double-exchange interaction between $\text{Co}^{3+}\text{--O--Co}^{4+}$ ^[34] cannot be denied completely especially because the ratio of Co^{3+} and Co^{4+} in this composition has been estimated as 2:1 in XPS analysis. Thus, in the present

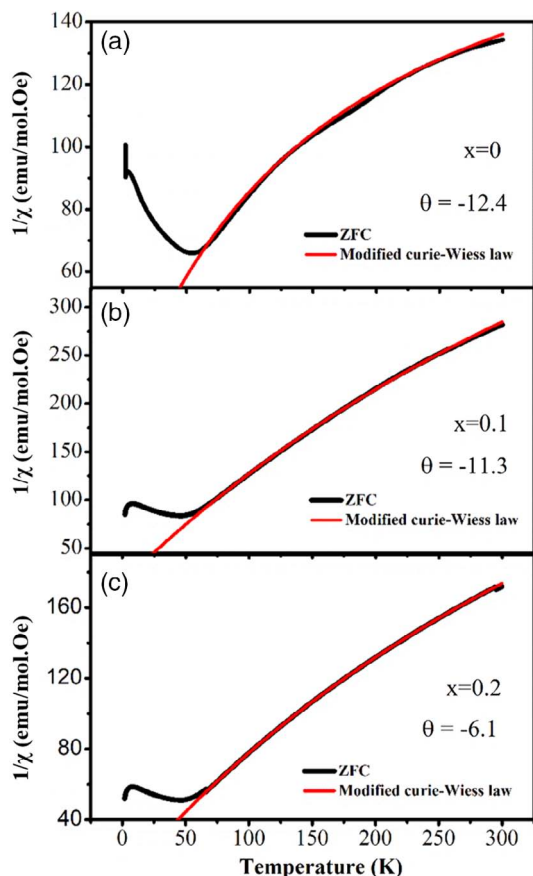


Figure 6. Modified Curie–Weiss law fitting for BSTC ($x = 0, 0.1,$ and 0.2) ceramic samples.

case, it can be hypothesized that, overall, antiferromagnetic-type coupling dominates over weak ferromagnetic coupling in the STC system. According to Goodenough–Kanamori rules,^[35] the superexchange interaction is antiferromagnetic where the electron transfers between overlapping orbitals that are each half filled. However, interaction is ferromagnetic, when electron

transfers from a half-filled to an empty orbital or from a filled to a half-filled orbital. The presence of antiferromagnetic and ferromagnetism in the system causes randomness and frustration between the spins, triggering spin-glass transition. Thus, BSTC ceramics exhibit locally coupled antiferromagnetic and weak ferromagnetic behavior, resulting in a spin-glass-like state.

The M – H curve for BSTC ($x = 0$ and 0.2) at 2 K shows a nonlinear behavior, as shown in **Figure 7**. The figure shows that M – H has nonzero remnant magnetization and a coercive field, although the values are very small. The M – H curve shows no saturation even at the high magnetic field (70 kOe), supporting the hypothesis for the presence of spin-glass-type behavior in BSTC samples.^[36]

To describe the unsaturated hysteresis loop of BSTC, we have considered two contributions, i.e., paramagnetic and ferromagnetic, defined as $M = M_1 + M_2$. The paramagnetic contribution can be written as $M_1 = \text{Constant}/T \times H$. However, ferromagnetic contribution M_2 determines the nature of the hysteresis loops. Geiler et al.^[37] proposed the following equation to describe the nonlinear hysteresis loop from ferromagnetic contribution

$$M_2(H) = \frac{2}{\pi} M_{\text{Sat}} \tan^{-1} \left[\frac{H - H_C}{H_T} \right] \quad (3)$$

where M_{Sat} is saturated magnetization, H is the external magnetic field, H_C is the coercive field, and H_T is a threshold field that has to be overcome to saturate the sample magnetically. The experimental curve is well fitted with Equation (1), as shown in **Figure 8**. The results of the fitted data of the experimental curves are shown in **Table 3**. It is shown in the table that BSTC ($x = 0.2$) shows a close value of H_T with the measured field as compared with pure STC, which requires a much higher magnetic field to obtain the saturation magnetization.

2.4. ESR Measurements of STC

To further understand the magnetic behavior of STC, ESR measurement has been carried out in the temperature range

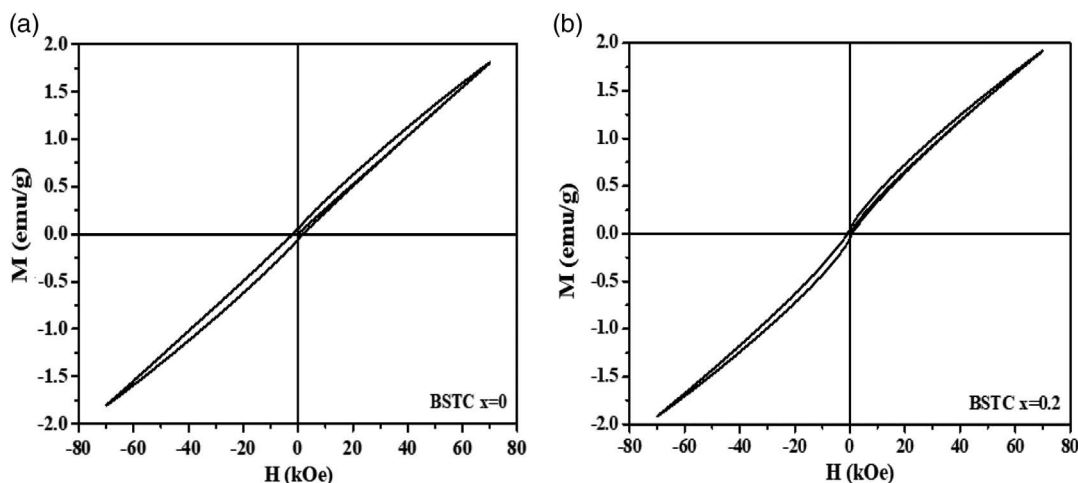


Figure 7. Magnetization versus magnetic field curve for $\text{Ba}_x\text{Sr}_{1-x}\text{TiCoO}_6$ with a) $x = 0$ and b) $x = 0.2$.

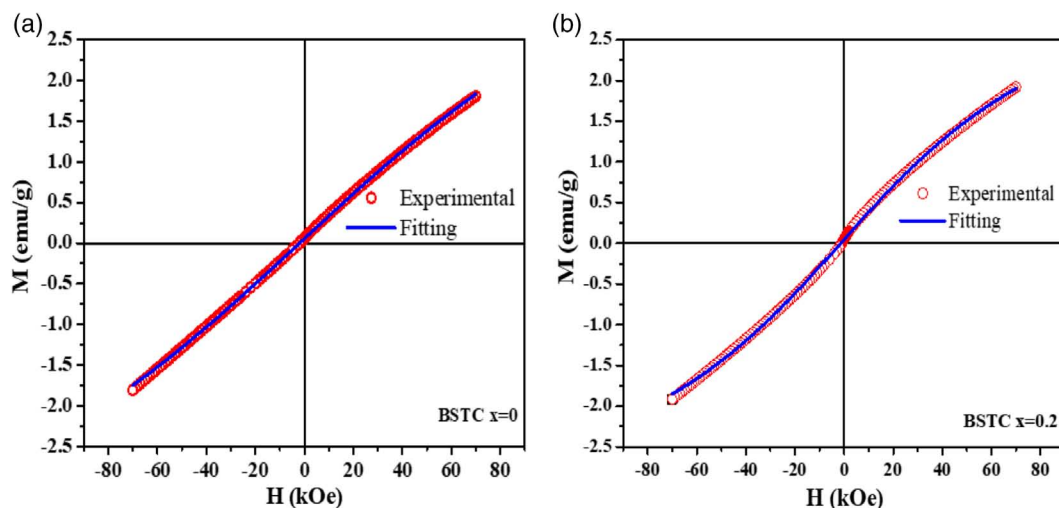


Figure 8. Magnetization versus magnetic field curve fitted with Equation (1) for $\text{Ba}_x\text{Sr}_{1-x}\text{TiCoO}_6$ with a) $x = 0$ and b) $x = 0.2$.

Table 3. The results of the fitted data of the experimental curves such as M_{Sat} , H_C , and H_T .

Composition	M_{Sat} [emu g^{-1}]	H_C [kOe]	H_T [kOe]
$x = 0$	5.62	1.99	128.388
$x = 0.2$	3.81	1.42	71.991

of 290–700 K at the magnetic field $B \leq 1.4$ T. Typical ESR spectra for the STC sample recorded at different temperatures are shown in **Figure 9**. Different parameters like resonance field (H_T) and linewidth (ΔH) have been obtained from fitting experimental lines. Figure 9a shows the temperature dependence of the ESR spectrum for pure STC samples. We have found that the ESR line can be adequately described by the sum of two components taken in Lorentzian form without any contribution of dispersion into

absorption. As the absorption line is relatively broad at high temperatures (of the same order as the resonance field), two circular components of the exciting linearly polarized microwave field have to be taken into account. ESR lines have been therefore fitted to the following formula^[38] in the conventional form.

$$\frac{dP}{dH} = \frac{d}{dH} \left(\frac{\Delta H + \alpha(H - H_0)}{\Delta H^2 + (H - H_0)^2} + \frac{\Delta H - \alpha(H + H_0)}{\Delta H^2 + (H + H_0)^2} \right) \quad (4)$$

where P is the power absorbed, H stands for a magnetic field, H_T is the resonance field, and ΔH represents the linewidth. The fitted curves have been found to be in excellent agreement with the experimental data. ESR lines consist of a superposition of two resonance modes, i.e., ferromagnetic and paramagnetic. Figure 9b shows the calculated ferromagnetic and paramagnetic contributions at some representative temperatures.

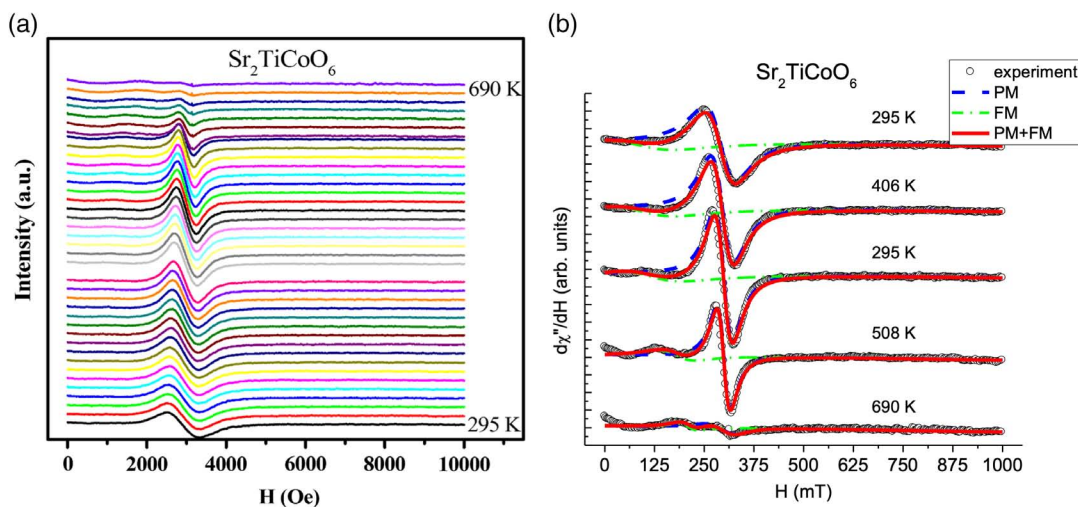


Figure 9. a) Temperature evolution of ESR line and b) the fitted ESR lines from the superposition of the calculated paramagnetic (PM) and ferromagnetic (FM) contributions for $\text{Sr}_2\text{TiCoO}_6$.

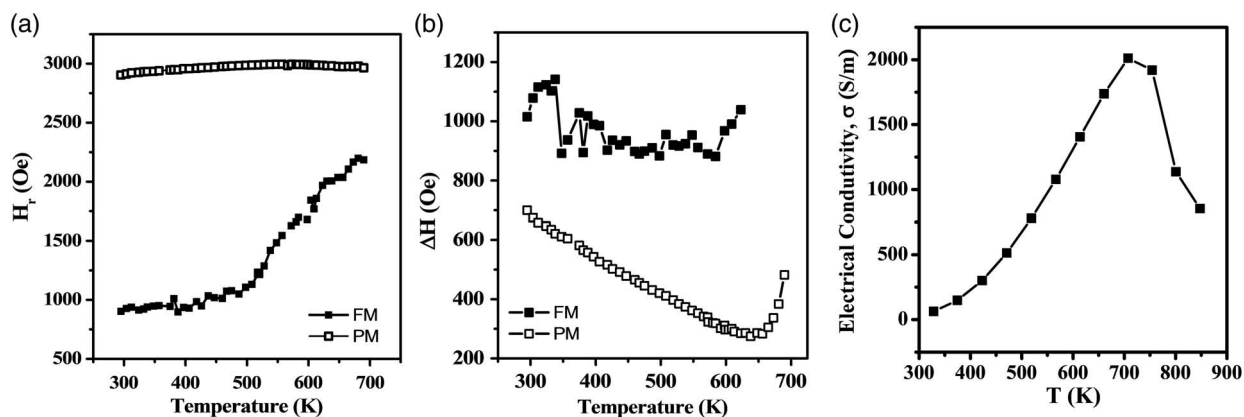


Figure 10. Temperature dependencies of ESR a) line resonance fields (H_r) and b) linewidth (ΔH) for $\text{Sr}_2\text{TiCoO}_6$, where solid symbols correspond to ferromagnetic contribution; c) electrical conductivity of $\text{Sr}_2\text{TiCoO}_6$.

Figure 10 shows the temperature dependence of the resonance field (H_r) and linewidth (ΔH) for STC samples. The paramagnetic line has been found to be almost temperature independent, whereas the ferromagnetic line has shown an increasing trend beyond 500 K, suggesting some kind of phase transitions in the system. Internal magnetic fields are supposed to be added to the external magnetic field. As a result, the ferromagnetic resonance line has been observed in a smaller magnetic field. It is believed that ferromagnetic contribution comes from the clusters of ferromagnetic ions in the samples.

A sudden increase in linewidth has been noted at about 650 K for the STC sample, which implies the possibility of a transition. Interestingly, at the same temperature (650 K), we have observed^[13] semiconductor ($d\sigma/dT > 0$) to metal ($d\sigma/dT < 0$) transition in the temperature-dependent electrical conductivity graph, as shown in Figure 10c. Linewidth is related to relaxation rate, which results from the balance of the broadening (dipolar) and narrowing (isotropic exchange) effects for strongly interacting spins.^[39] The larger linewidth is an indication of the smaller degree of exchange narrowing that can be described as Jahn–Teller ion behavior. Spin-glass behavior in STC is thought to be arisen because of uneven distribution of cobalt with multiple valence states in the sample. Jahn–Teller ions of cobalt (Co^{3+} , Co^{4+}) have different concentrations in different environments due to uneven distribution in the sample, making it difficult to identify a pattern. Analogous to spin glass where octahedral axis is randomly oriented, “Jahn–Teller glass” is possible^[40,41] to occur in this system. The reorientation of the long axis of octahedron may be responsible for possible tunneling and thermal transitions from one minimum to another.^[42] The existence of a composite spin-glass state (Jahn–Teller glass) is therefore proposed in STC, and the dynamic Jahn–Teller effect may be the possible mechanism behind the observed semiconductor ($d\sigma/dT > 0$) to metal ($d\sigma/dT < 0$) transition in electrical conductivity behavior.

3. Conclusions

In summary, BSTC double perovskite oxides have been prepared via the solid-state reaction method. XPS measurement shows the

presence of multivalent oxidation states of Co and Ti cations as Co^{3+} , Co^{4+} , Ti^{3+} , and Ti^{4+} . The Co^{3+} ($t_{2g}^5 e_g^1$) cations are predicted to reside in the IS state, whereas Co^{4+} ($t_{2g}^5 e_g^0$) is predicted to acquire an LS state. These BSTC double perovskites exhibit locally coupled antiferromagnetism and weak ferromagnetism, resulting in spin-glass-like behavior in the low-temperature magnetic measurement. ESR measurements further suggest the occurrence of Jahn–Teller glass analogous to the spin-glass behavior in STC ceramics, which has been attributed as the reason behind semiconductor-to-metal transition observed in temperature-dependent electrical conductivity behavior.

4. Experimental Section

Polycrystalline samples of BSTC ceramics were prepared via the conventional solid-state mixing route. SrCO_3 (Sigma-Aldrich $\geq 99.9\%$), Co_3O_4 (Sigma-Aldrich $> 99.5\%$), and TiO_2 (Sigma-Aldrich 99.5%) were used as starting materials. Stoichiometric amounts of raw materials were mixed using ball mill with zirconia balls. Powders were calcined in air at 1273 K for 10 h. Calcined powders were again ball milled in a planetary micromill (Fritsch, PULVERISETTE 7 premium Line, Germany) in an alcohol medium using zirconia grinding balls. Cylindrical samples (dimension $\approx 1.5 \times 13$ mm) were prepared using a uniaxial press. Compacted samples were then sintered in air at 1473 K for 12 h. XPS spectrum was conducted by PHI 5000 Versaprobe II using nonmonochromatic Al K α radiation that was used as an excitation source ($h\nu = 1486.6$ eV). Pressure inside the spectrometer was around 10^{-7} Pa. The magnetic properties of double perovskite samples were measured by using Quantum Design MPMS 3 (Indian Institute of Technology BHU, India). The temperature-dependent magnetic moment of ceramic samples was measured in the temperature range from 2 to 300 K under 300 Oe applied magnetic field in both field-cooled (FC) and zero-field-cooled (ZFC) conditions. Furthermore, field-dependent isothermal magnetization was measured at 2 K between +70 and –70 kOe. ESR measurements were conducted on a Varian E-12 spectrometer ($f = 9.4$ GHz) in the temperature range of 290–700 K at the magnetic field $B \leq 1.4$ T. The spectrometer was equipped with a flow nitrogen cryostat (Oxford Instruments) operating in the temperature range of 290–700 K.

Acknowledgements

This work was supported by the grant from Science and Engineering Research Board, DST (SERB-DST), India (grant nos. IMP/2018/000955 and SB/S3/ME/008/2015). The ESR spectra were measured within the

framework of fundamental research AAAA-A18-118030690040-8 at FRC Kazan Scientific Center of RAS.

Conflict of Interest

The authors declare no conflict of interest.

Keywords

double perovskites, electron spin resonance, magnetism, spin glass, $\text{Sr}_2\text{TiCoO}_6$

Received: June 14, 2019

Revised: January 6, 2020

Published online: January 30, 2020

- [1] M. D. C. Viola, M. Martinez-Lope, J. Alonso, P. Velasco, J. Martinez, J. Pedregosa, R. Carbonio, M. Fernandez-Diaz, *Chem. Mater.* **2002**, *14*, 812.
- [2] K.-I. Kobayashi, T. Kimura, H. Sawada, K. Terakura, Y. Tokura, *Nature* **1998**, *395*, 677.
- [3] Y. Lin, X. Chen, X. Liu, *Solid State Commun.* **2009**, *149*, 784.
- [4] O. N. Meetei, O. Erten, A. Mukherjee, M. Randeria, N. Trivedi, P. Woodward, *Phys. Rev. B* **2013**, *87*, 165104.
- [5] O. Erten, O. N. Meetei, A. Mukherjee, M. Randeria, N. Trivedi, P. Woodward, *Phys. Rev. B* **2013**, *87*, 165105.
- [6] T. Saha-Dasgupta, *J. Supercond. Novel Magn.* **2013**, *26*, 1991.
- [7] C. Ritter, M. Ibarra, L. Morellon, J. Blasco, J. Garcia, J. De Teresa, *J. Phys.: Condens. Matter* **2000**, *12*, 8295.
- [8] M. Sanjuán, M. Laguna, *Phys. Rev. B* **2001**, *64*, 174305.
- [9] M. Retuerto, M. Garcia-Hernandez, M. Martinez-Lope, M. Fernandez-Diaz, J. Attfield, J. Alonso, *J. Mater. Chem.* **2007**, *17*, 3555.
- [10] D. Serrate, J. De Teresa, M. Ibarra, *J. Phys.: Condens. Matter* **2006**, *19*, 023201.
- [11] J.-W. G. Bos, J. P. Attfield, *Phys. Rev. B* **2004**, *70*, 174434.
- [12] S. Kumar, G. Giovannetti, J. van den Brink, S. Picozzi, *Phys. Rev. B* **2010**, *82*, 134429.
- [13] M. Saxena, P. Roy, M. Acharya, I. Bose, K. Tanwar, T. Maiti, *Appl. Phys. Lett.* **2016**, *109*, 263903.
- [14] W. Meevasana, X. Zhou, B. Moritz, C. Chen, R. He, S. Fujimori, D. Lu, S. Mo, R. Moore, F. Baumberger, *New J. Phys.* **2010**, *12*, 023004.
- [15] S. Malo, A. Maignan, *Inorg. Chem.* **2004**, *43*, 8169.
- [16] S. Shtrikman, E. Wohlfarth, *Phys. Lett. A* **1981**, *85*, 467.
- [17] T. Sugahara, M. Ohtaki, *Appl. Phys. Lett.* **2011**, *99*, 062107.
- [18] M. S. Marshall, D. T. Newell, D. J. Payne, R. G. Egdell, M. R. Castell, *Phys. Rev. B* **2011**, *83*, 035410.
- [19] O. Lobacheva, Y. Yiu, N. Chen, T. Sham, L. Goncharova, *Appl. Surf. Sci.* **2017**, *393*, 74.
- [20] S. Butt, W. Xu, W. Q. He, Q. Tan, G. K. Ren, Y. Lin, C.-W. Nan, *J. Mater. Chem. A* **2014**, *2*, 19479.
- [21] E. Meza, J. Ortiz, D. Ruíz-León, J. F. Marco, J. L. Gautier, *Mater. Lett.* **2012**, *70*, 189.
- [22] J.-C. Dupin, D. Gonbeau, H. Benqlilou-Moudden, P. Vinatier, A. Levasseur, *Thin Solid Films* **2001**, *384*, 23.
- [23] B. J. Tan, K. J. Klabunde, P. M. Sherwood, *J. Am. Chem. Soc.* **1991**, *113*, 855.
- [24] L. Er-Rakho, C. Michel, P. Lacorre, B. Raveau, *J. Solid State Chem.* **1988**, *73*, 531.
- [25] M. Pissas, G. Kallias, V. Psycharis, H. Gamari-Seale, D. Niarchos, A. Simopoulos, R. Sonntag, *Phys. Rev. B* **1997**, *55*, 397.
- [26] M. Pissas, V. Psycharis, C. Mitros, G. Kallias, D. Niarchos, A. Simopoulos, A. Kostikas, *J. Magn. Magn. Mater.* **1992**, *104*, 571–572.
- [27] L. Er-Rakho, N. Nguyen, A. Ducouret, A. Samdi, C. Michel, *Solid State Sci.* **2005**, *7*, 165.
- [28] B. Wang, P. Tong, Y. Sun, X. Zhu, Z. Yang, W. Song, J. Dai, *Appl. Phys. Lett.* **2010**, *97*, 042508.
- [29] S. Lin, D. Shao, J. Lin, L. Zu, X. Kan, B. Wang, Y. Huang, W. Song, W. Lu, P. Tong, *J. Mater. Chem. C* **2015**, *3*, 5683.
- [30] M. Itoh, I. Natori, S. Kubota, K. Motoya, *J. Phys. Soc. Jpn.* **1994**, *63*, 1486.
- [31] J. Wu, C. Leighton, *Phys. Rev. B* **2003**, *67*, 174408.
- [32] Z. Liu, T. Waki, Y. Tabata, H. Nakamura, *Phys. Rev. B* **2014**, *89*, 054435.
- [33] G. Cao, S. McCall, M. Shepard, J. Crow, R. Guertin, *Phys. Rev. B* **1997**, *56*, 321.
- [34] J. Wu, C. Leighton, *Phys. Rev. B* **2013**, *67*, 174408.
- [35] J. B. Goodenough, *Scholarpedia* **2008**, *3*, 7382.
- [36] R. Pradheesh, H. S. Nair, C. Kumar, J. Lamsal, R. Nirmala, P. Santhosh, W. Yelon, S. Malik, V. Sankaranarayanan, K. Sethupathi, *J. Appl. Phys.* **2012**, *111*, 053905.
- [37] A. Geiler, V. Harris, C. Vittoria, N. Sun, *J. Appl. Phys.* **2006**, *99*, 08B316.
- [38] J. P. Joshi, S. Bhat, *J. Magn. Reson.* **2004**, *168*, 284.
- [39] M. Causa, A. Butera, M. Tovar, J. Fontcuberta, *Physica B* **2002**, *320*, 79.
- [40] M. Heinrich, H.-A. K. von Nidda, A. Krimmel, A. Loidl, R. Eremina, A. Ineev, B. Kochelaev, A. Prokofiev, W. Assmus, *Phys. Rev. B* **2003**, *67*, 224418.
- [41] M. Heinrich, H. A. K. von Nidda, R. Eremina, A. Loidl, C. Helbig, G. Obermeier, S. Horn, *Phys. Rev. Lett.* **2004**, *93*, 116402.
- [42] K. I. Kugel, D. Khomskii, *Physics-Uspeski* **1982**, *25*, 231.